

Article

Toward an Integrated and Sustainable Water Resources Management in Structurally-Controlled Watersheds in Desert Environments Using Geophysical and Remote Sensing Methods

Mohamed Attwa^{1,2}, Mohammed El Bastawesy², Dina Ragab³, Abdullah Othman^{4,5}, Hamza M. Assaggaf^{4,6} 
and Abotalib Z. Abotalib^{2,7,*} 

- ¹ Department of Geology, Zagazig University, Zagazig 44519, Egypt; attwa_m@zu.edu.eg
² Division of Geological Applications and Mineral Resources, National Authority of Remote Sensing and Space Sciences, Cairo 11843, Egypt; bastawesy_mmm@yahoo.com
³ Department of Geology, National Research Center, Cairo 12622, Egypt; dinaabdelmoeim@u.boisestate.edu
⁴ Natural Hazards Research Unit, Department of Environmental and Health Research, Umm Al-Qura University, Makkah 21955, Saudi Arabia; agothman@uqu.edu.sa (A.O.); hmsaggaf@uqu.edu.sa (H.M.A.)
⁵ Department of Environmental Engineering, Umm Al-Qura University, Makkah 21955, Saudi Arabia
⁶ Department of Laboratory, Umm Al-Qura University, Makkah 21955, Saudi Arabia
⁷ Viterbi School of Engineering, University of Southern California, Los Angeles, CA 90089, USA
* Correspondence: afarag@usc.edu; Tel.: +1-2692-678-640



Citation: Attwa, M.; El Bastawesy, M.; Ragab, D.; Othman, A.; Assaggaf, H.M.; Abotalib, A.Z. Toward an Integrated and Sustainable Water Resources Management in Structurally-Controlled Watersheds in Desert Environments Using Geophysical and Remote Sensing Methods. *Sustainability* **2021**, *13*, 4004. <https://doi.org/10.3390/su13074004>

Academic Editors: Mariusz Sojka and Dariusz Młyński

Received: 6 March 2021

Accepted: 1 April 2021

Published: 3 April 2021

Publisher's Note: MDPI stays neutral with regard to jurisdictional claims in published maps and institutional affiliations.



Copyright: © 2021 by the authors. Licensee MDPI, Basel, Switzerland. This article is an open access article distributed under the terms and conditions of the Creative Commons Attribution (CC BY) license (<https://creativecommons.org/licenses/by/4.0/>).

Abstract: Sustainable water resources management in desert environment has yet to be reached due to the limited hydrological datasets under such extreme arid conditions. In the Eastern Sahara, the tectonic activity associated with the opening of the Red Sea adds more complexity to developing sustainable water management by creating multiple aquifers within subsided half-grabens along the Red Sea extension. To overcome these difficulties, a two-fold approach is adopted including integrated remote sensing and geoelectrical methods using Wadi Al-Ambagi watershed in the Eastern Desert of Egypt as a test site. First, the total discharge is estimated as $15.7 \times 10^6 \text{ m}^3$ following the application of a uniform storm of 10 mm effective precipitation, which exceeds the storage capacity of existing mitigation measures ($5.5 \times 10^6 \text{ m}^3$), and thus additional dams are required. Second, the subsurface geometry of alluvium and sedimentary aquifers, within subsided blocks in the Arabian–Nubian shield (ANS), is delineated using 1D direct current and 2D electrical-resistivity tomography (ERT). Findings indicate that significant thicknesses of more than 80 m of permeable sedimentary units occur within the subsided blocks. Therefore, the scarce water resources can be managed by controlling the flash floods and suggesting proper dam sites at the location of thick alluvium and sedimentary rocks, where aquifers can be recharged representing a sustainable source for freshwater. The proposed approach is transferable and can be applied in similar arid rift-related watersheds in Saudi Arabia and worldwide.

Keywords: DC resistivity soundings; continental rift; flash floods; wadi systems; Egypt

1. Introduction

The opening of the Red Sea during the late-Oligocene–early-Miocene time as a major continental rift with a later transition to oceanic rift [1], resulted in the formation of extensional rift basins and half-grabens such as the Gulf of Suez and El-Qaa plain [2–4] as well as NW elongated gorges that modulated the east–west river flow, captured surface water, and introduced new northwest and north-flowing river systems [5]. The Red Sea opening also associated with significant uplift of the Arabian–Nubian shield (ANS) leading to erosion of enormous thicknesses of pre-rift Cambrian to Eocene rocks of up to 15 km [6,7], which ultimately resulted in the outcropping of the Precambrian crystalline rocks of the

ANS in the Eastern Desert of Egypt, Sinai, and western Saudi Arabia (Figure 1). In addition to the formation of major rift basins and half-grabens (Figure 1b), the extensional stresses also resulted in the preservation of pre-rift sedimentary successions in subsided blocks within the Precambrian ANS and near the coastal plain of the Red Sea, where relatively enhanced precipitation is taking place under the current arid climates [8]. Example of these subsided blocks include Jabal Duwi, Esh Al-Malaha in Egypt [2], and the Hamd-Jizl basin in Saudi Arabia [9]. However, these subsided blocks of sedimentary facies can be easily differentiated from the surrounding crystalline rocks on satellite images by their higher albedo (Figure 1c), yet some of these blocks are currently concealed beneath alluvium deposits within the major watersheds in the ANS. The storage capacity of these sedimentary rocks as well as the overlying alluvium, which is expected to attain significant thicknesses in subsided block areas, can be utilized as aquifers for flash-flood water harvesting and would also provide an effective mitigation measure against the destructive impacts of flash flooding in such desert areas.

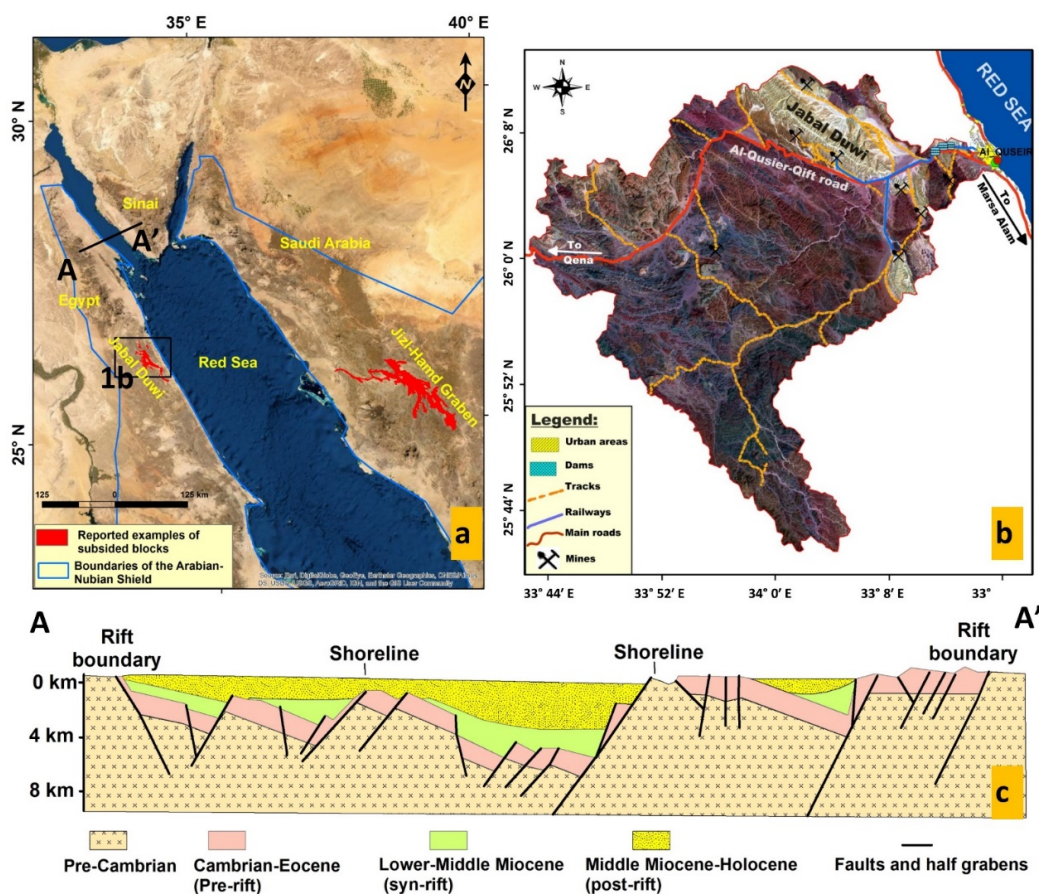


Figure 1. (a) Location map showing the boundaries of the Arabian–Nubian shield (ANS) and the location of subsided blocks within the ANS. (b) A simplified cross-section (along A–A' in 1a) showing the complex rift basins and half-grabens associated with the Red Sea opening, modified from [2]. (c) The test site of Wadi Al-Ambagi watershed showing the contrast between Jabal Duwi and the surrounding crystalline rocks of the ANS. The major roads and urban areas are also shown.

Remote sensing (RS) and geographic information system (GIS) have been increasingly used to improve the imitative methods of data collection in geological and environmental applications [10–13]. The problem of data limitation has been overcome as megascopic observations through available satellite images and digital elevation models (DEM) of different sources and resolutions [14–16]. As a main product of the shuttle radar topographic mission (SRTM), the DEM has been widely used for defining watershed characteristics [14,17], such as flow pathways and their confluences/dispersions and the estimation

of linear relationship of these networks [13]. The active channel detection and river flood-plains cross-sectional areas can be also estimated using high-resolution DEM data [18]. Recently, the morphometric analysis of watersheds is being conducted using the parameters obtained from remote sensing and GIS data [19]. There is a general agreement that examining the morphometric parameters of drainage systems is essential for understanding basin hydrogeological characteristics [18]. The hydrological analyses and management of flash floods can benefit from the qualitative and quantitative parameters obtained from RS and GIS data. Although, quantitative data on groundwater cannot be inferred from surface observations, but specific RS-based geological analyses can be integrated with geophysical exploration to assess the groundwater potentiality in different settings [20,21]. Moreover, the spatial analysis of these datasets in a GIS environment would improve the outcomes of such integrated analyses [22,23].

Traditionally, drilling is the first choice for subsurface site investigations given that it provides high accuracy and resolution at any required depths. Nevertheless, the borehole drillings are time consuming and expensive, and they only give point information. On the other hand, the surface geophysical methods give a timely effective and continuous imaging of subsurface layers including the depth to water table and the thickness of aquifers in the form of 1D, 2D, and 3D profiles [24,25]. The direct current resistivity (DCR) method is widely used for hydrogeophysical investigations [26,27]. The DCR sounding (1D) estimates directly the layer interfaces for groundwater exploration using 1D layered-model [28,29]. Moreover, the electrical-resistivity tomography (ERT) has been applied successfully for mapping the near-surface heterogeneities reflecting the subsurface structures, in a nondestructive manner [30]. Accordingly, the joint 1D and 2D DCR surveys can provide valuable information about the subsurface layer distributions and groundwater potentialities [31,32].

The present study aims to integrate RS observation/analyses, derivatives of DEM using GIS routines, and geophysical exploration in order to provide an integrated and sustainable water resources management in highly faulted watersheds in the ANS through (i) estimating the resultant runoff of designed storms, (ii) evaluating the extent of available alluvium and sedimentary aquifers, and (iii) examining the optimum scenario for runoff water harvesting and aquifer replenishment. To achieve these objectives the catchment of Wadi Al-Ambagi in the Eastern Desert of Egypt is selected as a test site. Existing mitigation measures are evaluated, and new measures are suggested to protect the urban areas downstream from flash-flood hazards. Furthermore, the exploration for alluvium and sedimentary aquifers suitable for groundwater accumulation is carried out using geophysical surveys being guided by hydrological and geological analyses for the sub-basins of the catchment.

2. Site Description

The Eastern Desert (ED) covers approximately 20% of Egypt. As a part of the eastern Sahara, the ED is dominated by arid to hyperarid conditions [33,34] and suffers from severe water scarcity. However, it has been recently hit by several flood events causing considerable economic damage and losses of life [35]. Wadi Al-Ambagi watershed represents a major connection corridor between the Nile Valley to the west and the Red Sea to the east via a paved road, Al-Quseir-Qift road (Figure 1c). The eastern part of the basin is formed of coastal plains, while the central and western areas include high relief mountainous (>100 m) terrains. The highest recorded rainfall on the watershed was 28 mm/year [36]. However, the basin has been subjected to frequent flash floods with reported seven flash-flood events during a period of twenty years (1996–2016) [35]. Further, it was observed that there is an extensive water shortage at the nearby Al-Qusier city for both domestic usage and mining operations. The existing mitigation measures include three constructed dams and a retention basin, which are mainly concentrated in the downstream part (Figure 1c), and consequently, their locations do not support aquifer recharge, i.e., runoff water harvesting (RWH).

The main streams are composed of interconnected relatively narrow meanders carved into mountainous areas and surrounded by high reliefs. The alignment of scarps overlooking the sectors of the main wadis is indicative of main structural control that conform variable depth to basement rocks underneath the wadi floors [35]. The impact of geological structures on wadi patterns, alluvium extent, and thickness is highly evident in the basin, where the grabens are occupied by alluvium of considerable thickness and saturation when compared with other stretches in the wadi floors that are covered by thin alluvium [37]. Numerous groups of faults were reported including the dominant NW–SE trend in addition to the NE–SW and E–W trends (Figure 2).

The geological setting of Wadi Al-Ambagi watershed is complex and the rock units range from Precambrian to Holocene. Precambrian rocks are exposed in the western parts of the watershed and are represented by wide variety of crystalline rocks (Figure 2) including migmatites, gneisses, calc-alkaline granite, metasediments, metavolcanics, mafic intrusions, younger volcanics, post-tectonic granites, and trachyte sheets and plugs [38]. Overall, the basement rocks are impermeable and may contain secondary porosity and permeability via fracturing particularly within the metavolcanic and sheared rock units [39]. The Precambrian units are unconformably overlain by sedimentary rock units. Cretaceous (shale, silt, Nubian sandstone, variegated shales, dark phosphate with silicified phosphatic nodules, marl, and limestone) and Eocene (shale and chalky limestone) rocks are exposed in Jabal Duwi area (Figure 2). Both the basement and Eocene sedimentary rocks are highly fractured by mostly connected joints and cracks while the Cretaceous Nubian sandstone and the Oligocene Nakheil sediments are less fractured, but their primary porosity and permeability make them among the main potential aquifers in the area [35]. Oligocene sediments consist mainly of coarse conglomerate alternating with bright variegated lacustrine calcareous clays [40]. The Red Sea coast is occupied by sediments related to the Miocene and Quaternary units (Figure 2). They unconformably overlie the older rocks with a distinctive dip. The Miocene deposits are distinguished as reefal and algal carbonate rocks, gypsiferous limestone rich in fossils, and sandstones with minor marls [40]. The Quaternary deposits appear as elevated beaches, alluvial fans, and wadi deposits. The wadi deposits are of different compositions according to the surrounding rock types [40]. The alluvium wadi deposits represent the main aquifer in the area as they receive occasional recharge from flash-flood events.

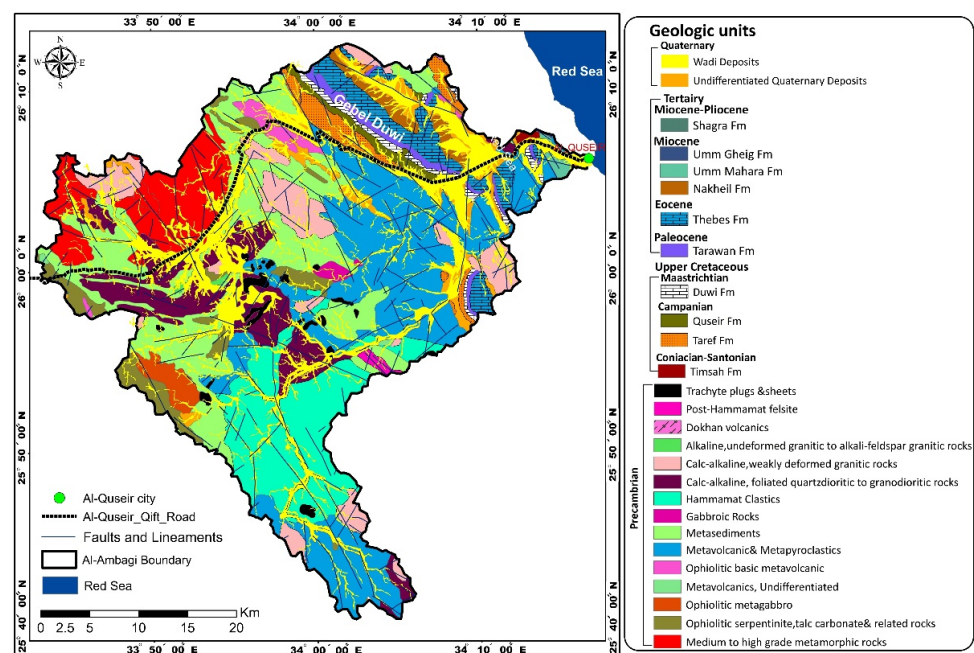


Figure 2. A geological map of Wadi al-Ambagi watershed showing different lithological and structural units, modified from [35,40].

3. Materials and Methods

3.1. Approach Overview

A two-fold approach for scarce water resources management and flash-flood hazard mitigation in structurally-controlled watersheds is presented in this study (Figure 3). First, surface and input data were collected, based on analysis of satellite data and field observations (stage I). In this stage, the storage capacities of existing mitigation measures were determined. Various topographic, morphometric, and hydrologic parameters were derived from RS datasets using Envi 5.1, ArcGIS 10.2, and ERDAS Imagine. The corresponding total discharge of the whole basin (i.e., hydrograph) was then calculated. Consequently, the difference between the estimated total discharge and the storage capacity of the existing mitigation measures were examined, and thus additional mitigation measures were recommended. Second, the subsurface data were acquired from borehole data and DCR measurements, in the form of DC resistivity soundings and 2D-ERTs (stage II). Given that the inverse problem of DC resistivity data is usually ill posed, advanced conventional and nonconventional algorithms were applied to improve the interpretation results. The aim of DCR soundings is to (i) attain a general overview of subsurface layers distribution and (ii) evaluate the hydrogeological conditions. The distribution of geophysical measurements was controlled by results of stage I, e.g., surface geological data and locations of the main wadis. Finally, the results of stages I and II were integrated to get proper solutions/locations for improve runoff water harvesting and aquifer replenishment, which are necessary for sustainable water management in wadi systems under hyperarid conditions.

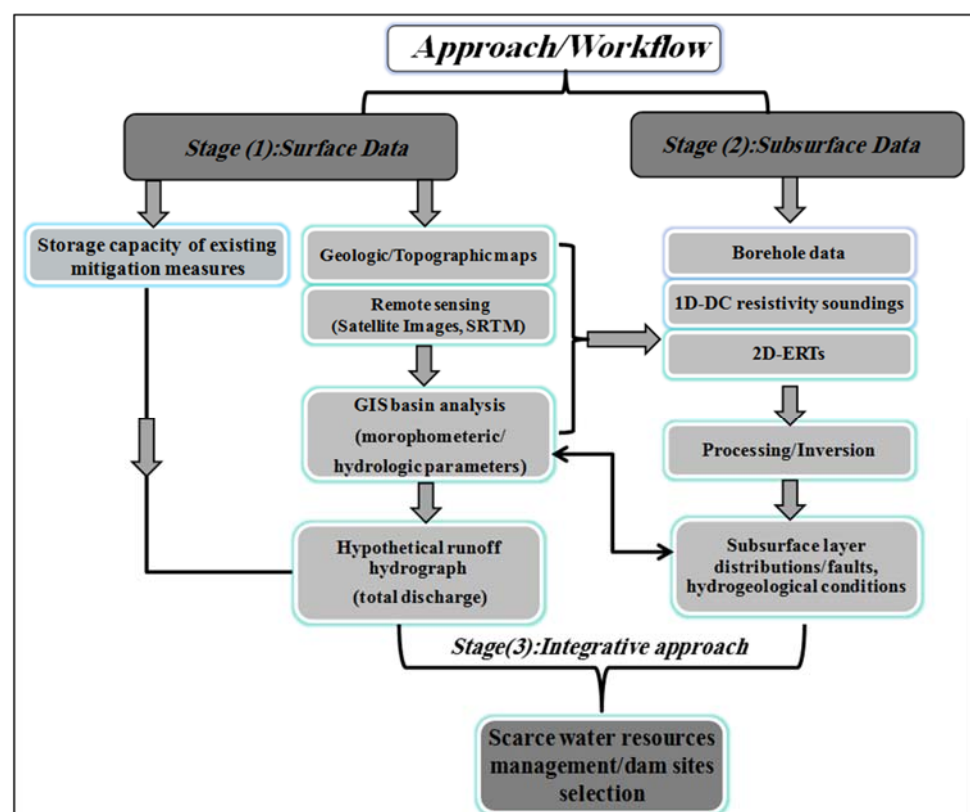


Figure 3. Integrated flowchart of the proposed approach for scarce water resources management in dryland basins.

3.2. Extraction of Surface Hydrological Parameters (Stage I)

Based on field observations, the existing mitigation measures have been evaluated. The storage capacity of observed dams and pools were measured to estimate the amount of retained water. Given that the watershed is inactive for long periods except during

intensive rain storms, there are no available field measurements such as flow records and ancillary data. This lack of information impedes the full understanding of the processes associated with flash floods and the calibration of estimated flow parameters. Therefore, the flash-flood modeling is of utmost importance to help the planners and executives not only to mitigate the negative impact but also to gain benefit from these occasional flows.

The available topographic maps were geographically rectified and mosaicked, and the catchment boundary was delineated in a GIS environment. The different layers on the topographic maps were digitized including: contours, elevation points, stream networks, and land cover features. These datasets were integrated to examine the accuracy of the shuttle radar topography mission (SRTM)-derived DEM (Figure 4a) as well as for hydrological analyses.

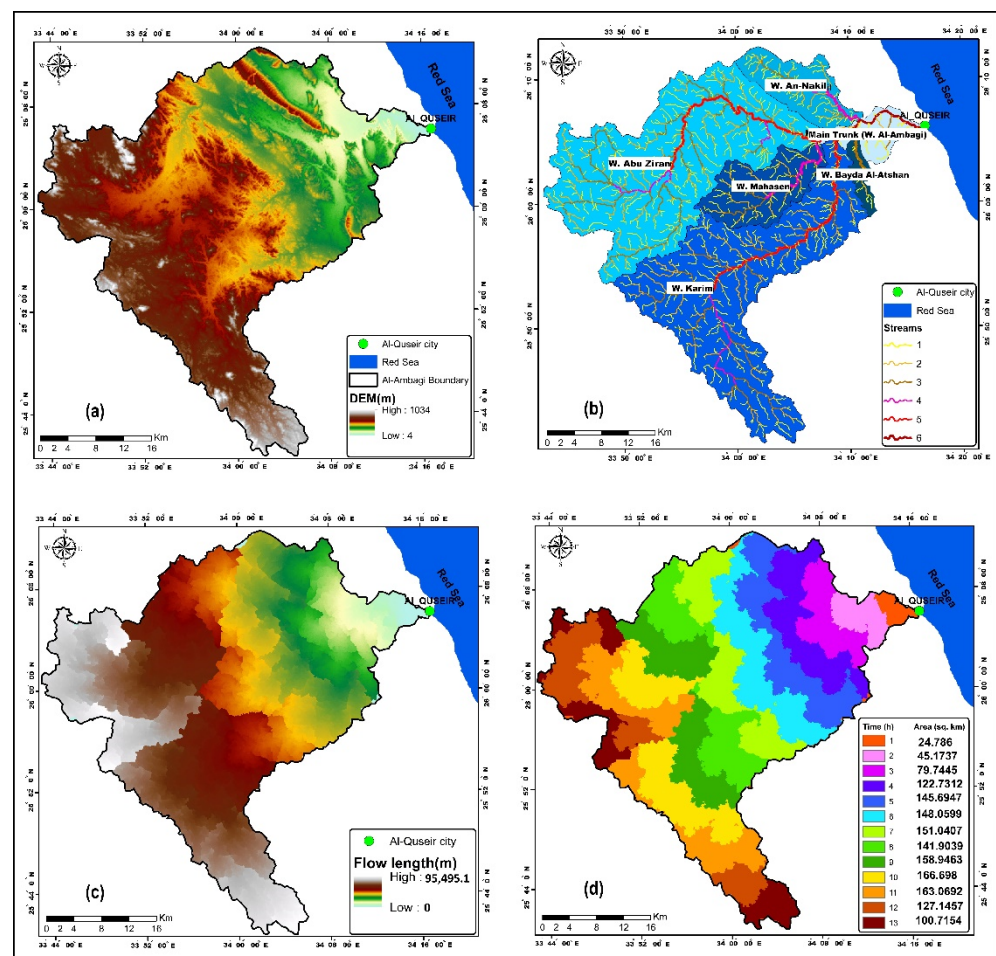


Figure 4. Different data layers used in the assessment of water resources; (a) digital elevation models (DEM) in (m), (b) sub-basins and drainage network, (c) flow length in (m), and (d) the resulting time-area zones of the catchment that contribute to the resulting runoff successively toward the watershed outlet.

The main basin has been subdivided into six sub-basins named as Abu-Ziran (a), Karim (b), Mahasin (c), An-nakhil (d), the main trunk of wadi Al-Ambagi (e), and Bayda al-Atshan (f) sub-basins (Figure 4b). Most of these wadis debouch into the east toward the Red Sea coast, where urban areas, mining sites, and tourist villages are located (Figure 1c). Based on the DEM analyses, morphometric parameters of the basin were derived and then they were grouped as linear, relief, and areal parameters. Using the Manning equation, the overland and channel flow velocities were empirically estimated as:

$$V = (R^{0.67} S^{0.5}) / n \quad (1)$$

where V is the cross-sectional average velocity (m/s), R is the hydraulic radius (m), S is the slope of the water surface, and n is the Manning coefficient. The water surface slope is assumed to be parallel to the channel bed slope.

The channel width at selected sites was measured using active channel characteristics on the Landsat images acquired directly after flash-flood events over the watershed (i.e., high albedo). These selected cross-sections were then superimposed on the DEM to extract the average depth at each site. Slope of the water surface as a function of the channel bed slope was estimated from the DEM for reaches centered on the selected sites. Hydraulic radius was also calculated from the measured cross-sectional areas and perimeter. The Manning coefficient was considered as 0.02 for channel areas and 0.06 for hillslopes as typically reported for similar watersheds in the Eastern Desert of Egypt [17]. The extracted DEM were used to derive various hydrological parameters; i.e., flow direction using the D-8 algorithm, flow accumulation, watershed delineation, stream networks, downstream flow length (Figure 4c), and the time-area zones (Figure 4d). Given that the flow direction represents the direction of flow within each cell in the watershed and the pixel resolution of the utilized DEM is known, the cell flow length can be derived. With the known values of the flow velocities and the flow lengths, the travel time of flow in each cell can be directly estimated by dividing the flow length by the flow velocity. The catchment has been subdivided into sets of cascading time-area zones in order to compute the temporal distribution of resulting runoff on hourly basis. The time-area zones (Figure 4d), which represent the time required for the runoff generated at each cell to reach the outlet, were produced using the flow length function in ArcGIS.

3.3. Subsurface Data Acquisition/DCR Inversion (Stage II)

The subsurface data were acquired from available borehole and DCR data. Figure 5 shows the DCR measurement locations using SYSCAL R2, IRIS instrument. The DCR data were stacked taking into consideration the noise level. The apparent DCR data were stacked 10 times. The final data were registered when the data quality factor value was minimized (stacked error < 1%). The surface layer consists of Quaternary basement fragment and gravelly sand, which is characterized by very high-resistivity values causing a high resistance contact. Accordingly, stainless-steel electrodes with saltwater around a poor contact electrode were used to improve electrodes connection with near surface soil. Furthermore, the DCR sounding distribution was carried out based on the accessibility of the basin, where many mountains, queries, and hills are out of reach for geophysical measurements. Accordingly, the DCR soundings were arranged in an irregular pattern (Figure 5).

The field surveys were conducted through gradual stages from April 2015 until September 2016. The DCR measurements were subdivided into two main terms. The first one is the DCR sounding (i.e., 1D), and the other term is the 2D-ERTs. The resistivity measurements were carried out along the main wadi bed where the stream density is high to explore alluvium and sedimentary thickness, saturation, and depth to the basement rocks. To attain regional geological information, eighteen DCR soundings using Schlumberger array with 300 m maximum half-electrode spacing ($AB/2$) were measured as shown in (Figure 5).

After the DCR sounding data have been interpreted, two 2D profiles were acquired using Wenner beta array (Figure 5). Considering the results of stage (I) and DCR soundings interpretation, the 2D-ERT profiles were carried out in the wadi floor at two selected sites of complex structures, i.e., in areas being intercepted by structurally aligned scarps on opposite sides of the wadi. The 2D-ERTs (Figure 5) were acquired manually using 30 electrodes with 5 m electrode spacing for P1 (145 m length) and 6 m for P2 (174 m length). In view of Wenner beta configuration advantages [41], this array was selected for the 2D-ERT survey.

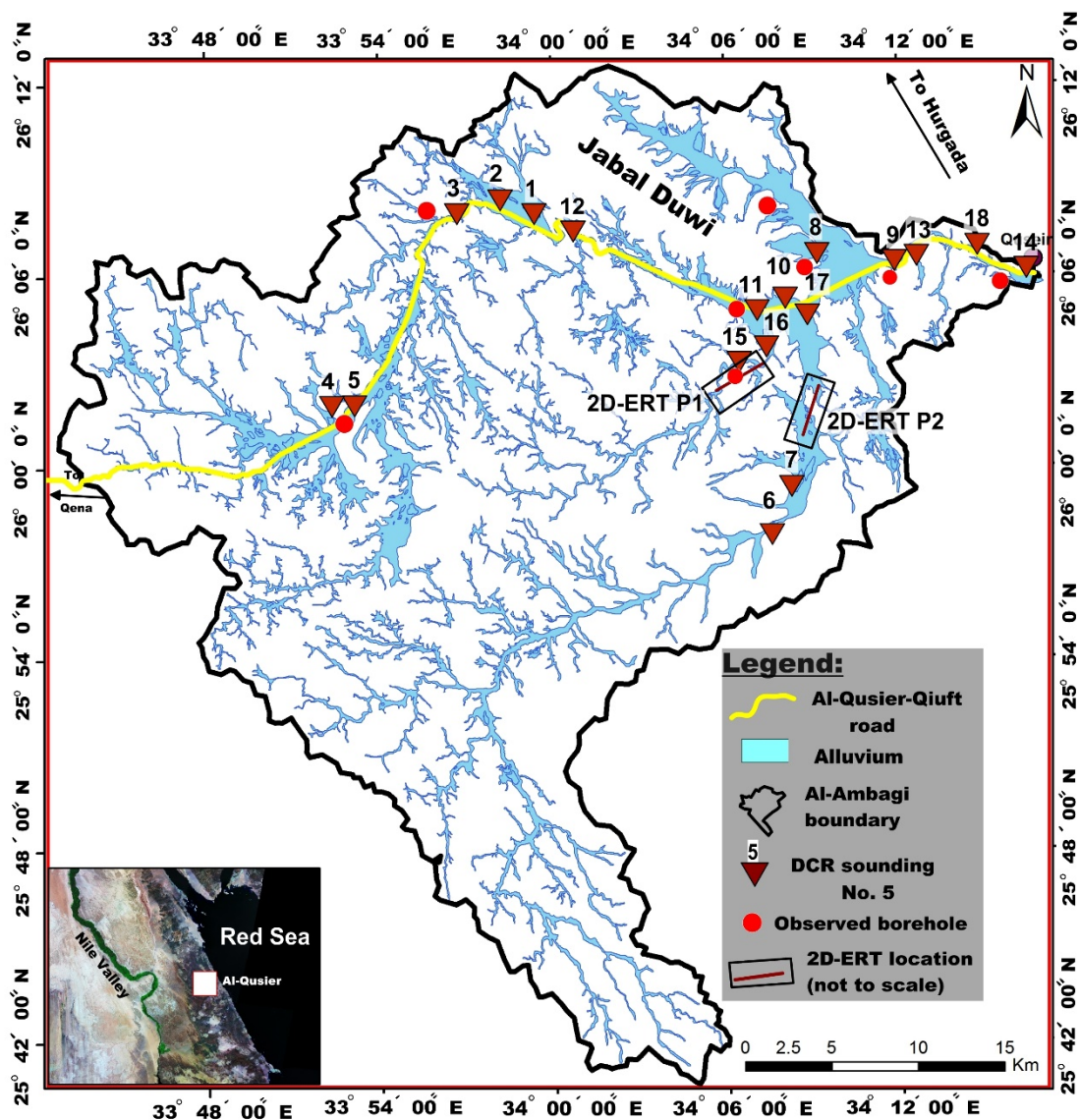


Figure 5. Locations of acquired geophysical measurement (1D-DCR (direct current resistivity) soundings and 2D-ERTs (electrical-resistivity tomography)) along the main streams in Wadi Al-Ambagi watershed.

To reduce the DCR interpretation uncertainty, the measurements were executed near to available boreholes (i.e., seven boreholes) (Figure 5). Based on Attwa and Henaish [41], a combined use of conventional and nonconventional inversion algorithms was applied. The DCR soundings were interpreted using a sequential inversion algorithm [42] applying damped least-squares algorithm (e.g., Levenberg–Marquardt). The measured sounding data points were smoothed applying 1D smoothness weighting schemes. Then, the nonconventional inversion procedure (genetic algorithms) was applied using a low misfit value heuristic search [43,44]. Regarding the sequential interpretation of [42] results and borehole data, the search space was adapted in the genetic algorithms.

Figure 6 shows the DCR sounding No. 15 inversion results. Notably, the generation number and population size were both 60. Then, all measured DCR soundings were inverted applying genetic algorithms and using the same number of generations and populations. Here, the available borehole data were considered to strengthen the inversion process, and consequently, the subsurface layer distributions, structures, and hydrogeological conditions can be delineated from the stitched-resistivity sections.

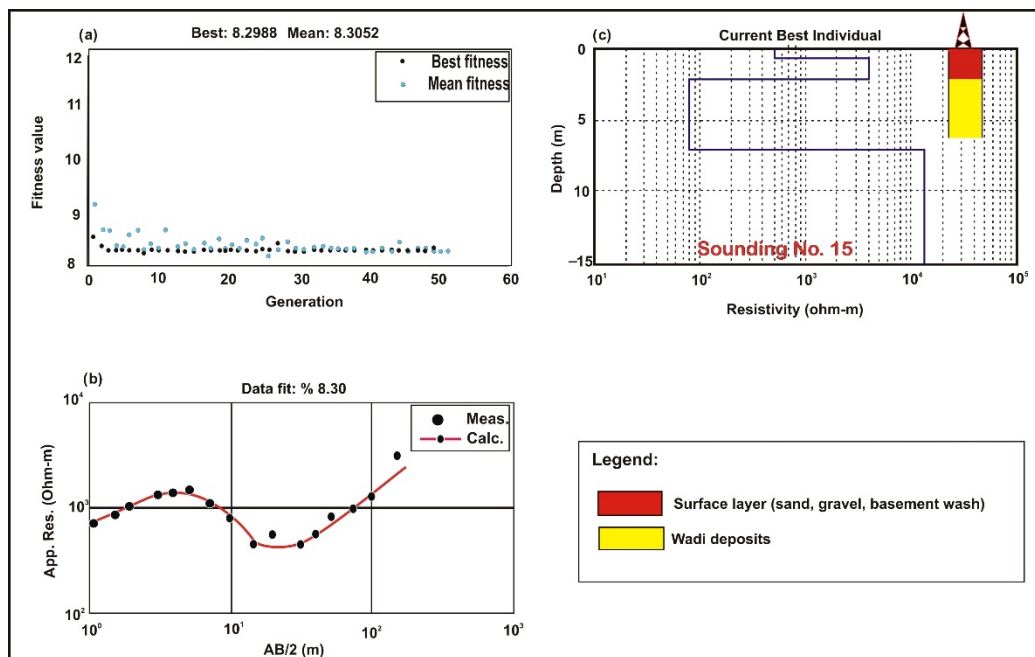


Figure 6. DCR sounding No. 15 (for location, c.f. Figure 2b) inversion results using genetic algorithms. (a) The mean and best misfit values versus generations. (b) The fitting between the measured and calculated-resistivity data. (c) Correlation between the layers intrinsic resistivity and the observed borehole information.

The 2D-ERTs were processed/inverted using a conventional derivative based inversion (DBI) method. Boundless Electrical-resistivity Tomography (BERT) software package was employed, which is widely used in geological/hydrogeological evaluation [45–47]. In case of DCR processing, the measured data were excluded for insignificant current and/or high standard deviation (>5%). The bad data quality of outliers and negative field data were rejected. The deleted data were not more than 6% of the measured resistivity data for each 2D-ERT. As suggested by many authors [41,48], an error level of 5% plus 10 μV was selected as the reciprocity data were not measured.

The inversion scheme of BERT depends on several meshes and finite-element forward modeling [49]. In BERT, the inversion method uses the Gauss–Newton algorithm with inexact line search using the methodology described in [48]. Because the watershed is characterized by rough topography, an unstructured mesh of irregular triangles was generated using Delaunay triangulation in forward calculation [49]. The variation between the field data and model response was minimized applying L2-Norm [48]. The 2D inversion implementation concerning a global regularization scheme was applied using a first-order smoothness constraint [49]. The artifact effects regarding the near-surface heterogeneities were minimized using different weights for, respectively, horizontal and vertical model boundaries, $a_x = \lambda$ (known as “LAMBDA”) and $a_z = \lambda w_z$ (called “ZWEIGHT”), were applied.

4. Results and Discussions

A hypothetical uniform rainstorm event was favorably utilized to assess the flash-flood hazards in Wadi Al-Ambagi watershed rather than using historical rainfall events. This is because of the limited hydrological datasets in desert watersheds with the overwhelming majority of the Saharan watersheds are ungauged [17] and given that the rainfall in such hyperarid environments is highly variable in time with the rainfall in one event can be more than 80 times the average annual precipitation [50]. Moreover, the rainfall over desert areas is highly localized in space, where, for any specific storms, rainfall measurements at stations just 2–3 km apart can differ by factors from 10 to 20 [51]. The time-area zone (Figure 4d) was calculated for Wadi Al-Ambagi watershed in order to estimate the unit

hydrograph (i.e., flash-flood discharge curve, Figure 7), which was derived depending on the methodologies proposed in Maidment [52] for the generation of a GIS-based spatially distributed unit hydrograph using a hypothetical effective runoff coefficient of 10 mm/h (i.e., rainfall excess) as suggested in El Bastawesy et al. [17]. This value is equivalent to the minimum streamflow initiation threshold in the North African Sahara that has been determined based on field measurements and was commonly used in flash-flood assessment in desert environments [17,53–55]. This rainfall event was supposed to be of homogeneous concentration over the whole basin, and the water flow was transmitted linearly to the downstream direction from each time zone on an hourly origin without transmission loss through the channel bed. According to the GIS-based spatially distributed synthetic unit hydrograph (Figure 7), the total discharge of the whole watershed has been calculated and summarized in Table 1. It is worth mentioning that these estimations represent a conservative estimate of the total discharge of the watershed, and thus any rainfall storm that exceeds 10 mm/h would yield a larger total discharge.

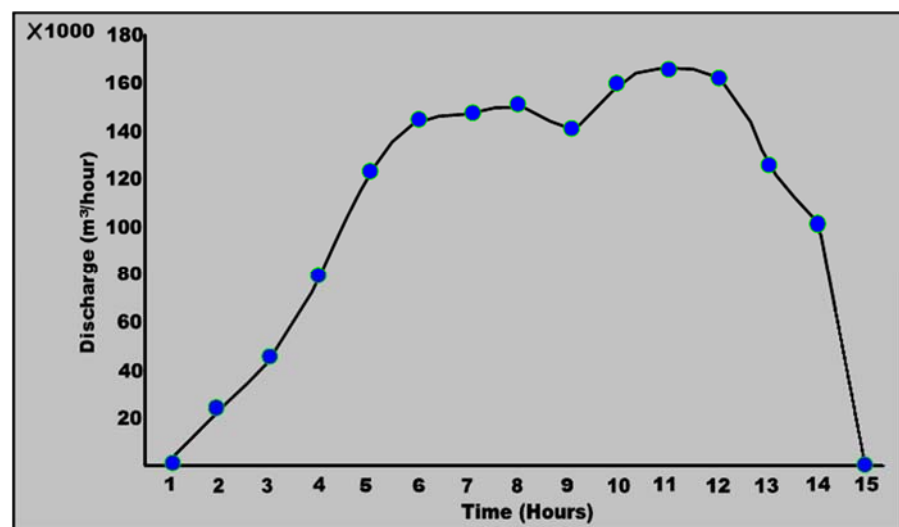


Figure 7. The hypothetical unit hydrograph that would result from a hypothetical 10 mm/h rainfall storm at wadi Al-Ambagi watershed.

Table 1. The estimated runoff parameters of Wadi Al-Ambagi sub-basins.

Name	Area (km ²)	Total Discharge (m ³)	Flow Duration (hours)	Peak Discharge Rate (m ³ /s)	Time to Peak (hour)	Impact
Wadi Abu-Ziran	615.6	6,349,995	12	119.835	9	Quseir-Qift road
WadiKarim	571.5	5,899,392	13	134.1563	8	Quseir-Qift road
Wadian_Nakhil	111.5	1,153,116	6	56.05875	3	Quseir-Qift road
Wadi Mahasen	137.8	1,427,868	6	60.46875	3	Quseir-Qift road
Wadi Bayda al Atshan	25.1	259,524	4	19.08	2	Quseir-Qift road
Total: Al-Ambagi Basin	1524.7	15,757,000	15	231.525	10	Quseir City

The total discharge amount produced from the whole watershed of Al-Ambagi has been estimated as 15.7×10^6 m³ (Table 1). On the other hand, the storage capacities of dams 1, 2, and 3 and the retention basin (Table 2), as measured in the field, were 0.4, 1.69, 2.7, and

$0.72 \times 10^6 \text{ m}^3$, respectively, yielding a total storage capacity of $5.5 \times 10^6 \text{ m}^3$. Therefore, the existing mitigation measures at the main trunk of Wadi Al-Ambagi watershed (Figure 1c) are not sufficient to fully protect Al-Quseir city and Al-Quseir-Qift road (Figure 1c) from severe flash floods. Consequently, further dams are required to (i) reduce the total discharge at the downstream part and (ii) recharge the aquifers to provide an optimum water resources management in the wadi system.

Table 2. Storage capacity of the existing mitigation measures.

Dams	Storage Capacity (m^3)	Total Storage Capacity (m^3)	Estimated Total Discharge (m^3)	Required Storage Capacity (m^3)
Dam-1	402,268			
Dam-2	1,695,956			
Dam-3	2,701,193	5,519,417	15,757,092	10,237,675
Pool	720,000			

In this work, the hydrogeological and structural models were constructed using new approaches after [41,56]. The interpretation of DCR data has been calibrated with surface and subsurface geological/structural data. In general, field observations and interpretation of satellite images and topographic maps have led to define major geological structures such as subsided blocks and faults. In order to obtain a regional overview of the distribution of subsurface layers, the inversion results of 18 sounding points were integrated in comparison with the available borehole data to construct geoelectrical cross-sections and a 3D schematic model (Figures 8 and 9). The fact that the sedimentary materials in the subsided blocks are mainly topped with Eocene, Oligocene, and Quaternary sediments implies that rift-related normal faulting is the main tectonic deformation in the study site [1–4], and thus folding is unlikely to be reported from such extensional rift systems [2,6]. The inferred faults considering to the displacement of geoelectrical layers on the constructed geoelectrical sections were correlated with the aerial distribution of outcropped geological units and the geometry of surface mapped faults. Such prior controls were considered in constructing the stitched-resistivity sections. Consequently, the misinterpretation of DCR data can be reduced using the abovementioned controls.

Inspection of the constructed stitched-resistivity sections (Figure 8) indicated that the majority of DCR soundings, located at wadis Abu Ziran and Mahasen, comprise three geoelectrical layers, which can be attributed to wadi deposits (surface layer) of wide range of resistivities (60–10,000 ohm-m) related to high-heterogeneity medium-resistivity layer (28–90 ohm-m) corresponding to saturated fractured basement and high-resistivity layer (>1000 ppm) regarding basement rocks. Toward the Red Sea (wadi Al-Ambagi), the surface layer is by very low (<5 ohm-m, DCR sounding No. 14) to very high (>2000 ohm-m, DCR sounding No. 18)-resistivity layers corresponding to Quaternary alluvium saturated with seawater (turquoise color) and Miocene salt rich terraces (pastel blue), respectively. At Wadi An-Nakhil (Figure 5), the inversion results of DCR soundings No. 8 and 9 (Figure 8 middle) represent four resistivity layers. According to the geological investigations and borehole information, the Oligocene rocks are dominant [35,51]. Accordingly, the surface layer (wadi deposits) is underlain, from top to bottom, by a low-resistivity layer (17–21 ohm-m) corresponding to Oligocene shale (red-brown color), a high-resistivity layer (>1000 ohm-m) attributing to Oligocene sandstone (light-yellow color), and a medium-resistivity layer (49–97 ohm-m) corresponding to saturated Nakheil sandstone aquifer (baby-blue color). Regarding the inferred fault between soundings No. 8 and 10, Nakheil sandstone aquifer is absent at sounding No. 10. At downstream portion of wadi Karim, the inversion results of DCR sounding No. 7 represent three geoelectrical layers. Thanks to calibration with observed borehole and geological data, the second resistivity layer (1278 ohm-m) can be attributed to the Nubian sandstone (light-yellow color).

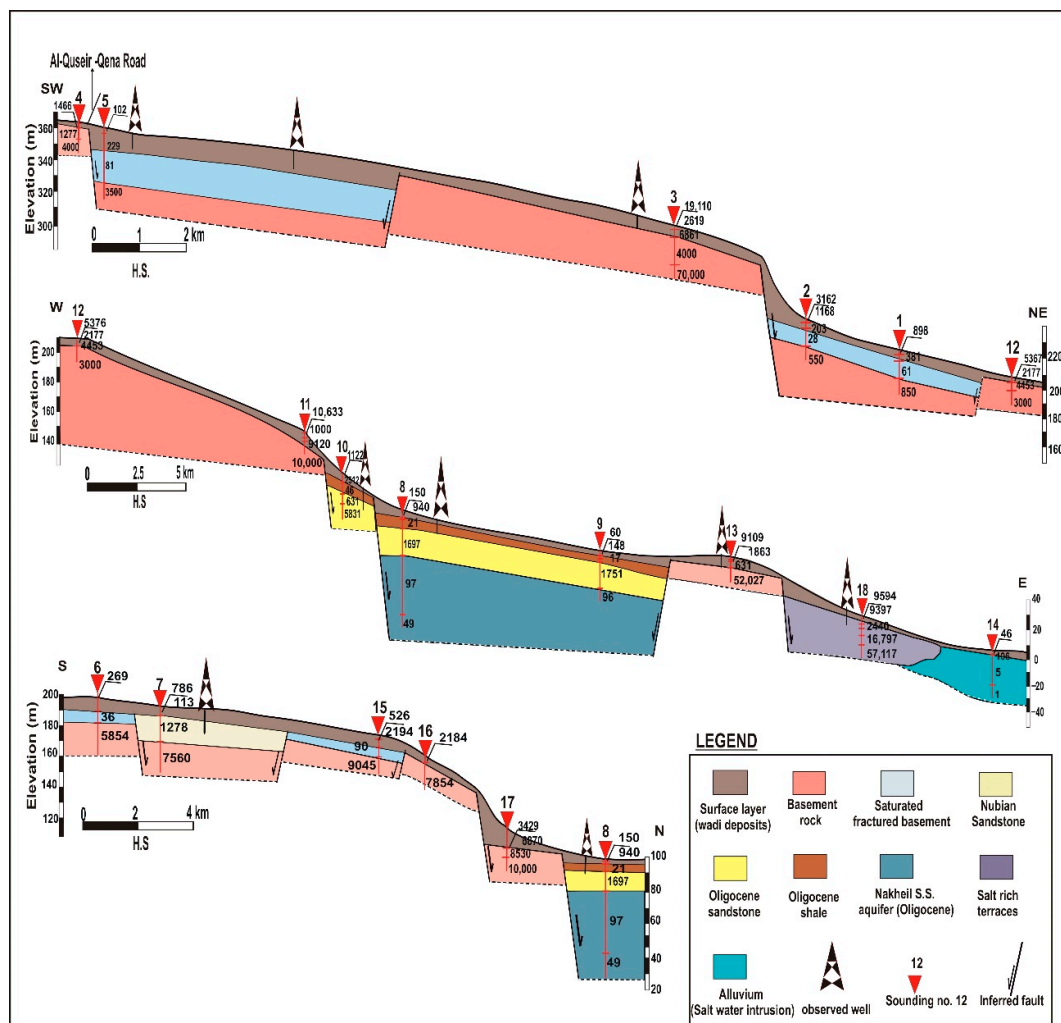


Figure 8. Stitched-resistivity sections derived from integration of inversion results of DCR soundings and available borehole/hydrogeological data.

The 3D schematic model (Figure 9) shows the general overview of geological and hydrogeological conditions at the central part of Wadi Al-Ambagi watershed passing through three sub-basins (wadis Abu Ziran, Al-Ambagi, and An-Nakhil). Inspection of Figure 9 showed that the regional structural setting plays an essential role in groundwater occurrences. The aquifers at the upstream portion (soundings No. 1, 2, and 5) are associated with fractured basement rocks with 10 m average thickness (Figures 9 and 10). Regarding previous hydrogeological studies [35], the basement rocks uplifting decreases groundwater potentialities by decreasing the fractured basement aquifer thickness. By contrast, the aquifers can be observed in graben structures within Oligocene Nakheil sandstone with considerable thickness at wadis Al-Ambagi and An-Nakhil (for location, c.f. Figure 4b). In comparison with the upstream portion aquifer (i.e., fractured basement rocks), the Oligocene aquifer is deeper (~60–70 m) and thicker (~>30 m). It is worth mentioning that the subsided blocks in the form of half-grabens that are associated with the Red Sea rifting (e.g., jabal Duwi (Figure 9)) preserved these considerable thicknesses of sedimentary layers and thus provided a significant opportunity for surface runoff water harvesting in these locations. These results are in general agreement with previous geological and hydrogeological studies carried by many authors [2,35].

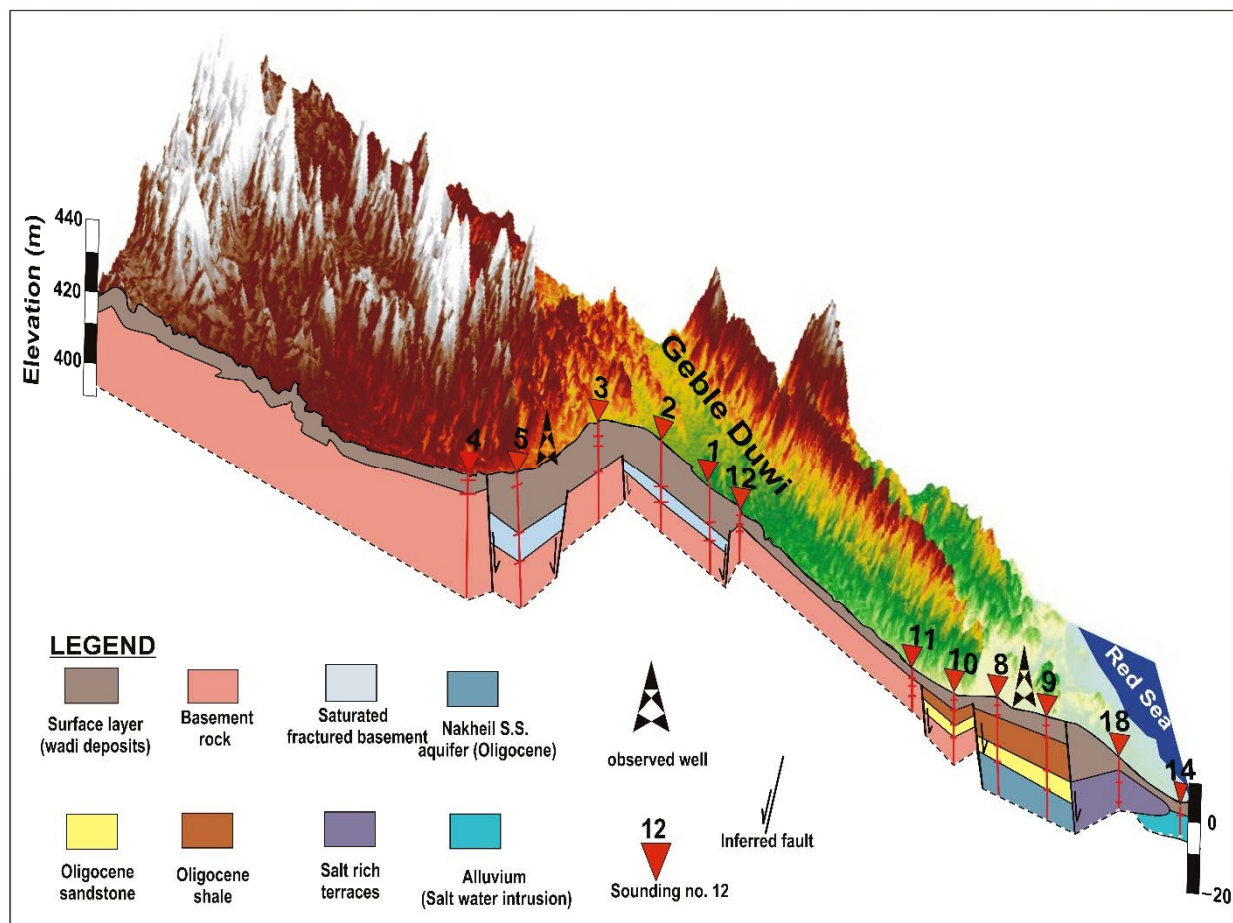


Figure 9. Stitched-resistivity section in the form of 3D schematic model showing the subsurface geological and hydrogeological conditions along Al-Quseir Qift desert road.

In order to better understand the subsurface setting in the subsided block areas, where significant thicknesses of permeable sedimentary rocks are determined from the DCR measurements, the 2D-ERT survey lines P1 and P2 (Figure 10a) were measured at right angle to the observed normal faults at wadis Mahasen and Bayda Al-Atshan, (Figure 5). Such 2D-ERTs calibrated with available borehole data and interpretation of DCR sounding No. 15 (Figure 10a). The 2D-ERTs P1 and P2 show detailed information on the subsurface faults and their consequence on the juxtaposing rock units. Inspection of the 2D-ERTs of P1 and P2 shows that the subsurface is dominated by two main geoelectrical layers. The first layer shows high-resistivity values (>1000 ohm-m) corresponding to basement rocks/debris. The second layer shows medium-resistivity values (100–200 ohm-m), which can be related to saturated wadi deposits (saturated alluvium). Considering the observed regional fault locations (Figure 10a), normal faults were recalled and projected into the 2D-ERTs P1 and P2 (Figure 10d and e, respectively). Accordingly, truncation of low-resistivity zone against high-resistivity zone along 2D-ERTs P1 and P2 can be associated with normal faults as indicated by the regional structural observations [2–6]. These geological conditions indicate opportunity to recharge the aquifer (alluvium and underlying sedimentary rocks) through constructing two dams to harvest flash-flood water at these locations. These locations (Figure 10) are also characterized by suitable topographic settings, where the wadis are narrow and bounded by elevated terrains of impermeable crystalline rocks, and on the other hand, they cut through high permeable sedimentary layers and high annual transmission loss rates of up to 28% of annual precipitation [57]. These characteristics increase the potentiality of water percolation to the aquifers in the subsided blocks. If a proper management plan of these dams is adopted to avoid significant evaporation from their

ponds, the accumulated water can recharge the aquifers either through natural infiltration or through recharge wells. Ultimately, the flash-flood hazards at the downstream portion of Wadi Al-Ambagi watershed can be managed and mitigated. This harvesting mechanism will be effective due to the existing underground basement blocks and structures which can control the water movement and contain the water within the subsided blocks upstream, and thus, the stored water can be regularly extracted and supplied to the nearby Al-Qussier city and the mining sites. The impact of building these dams on the ecosystem in Wadi Al-Ambagi watershed and the rate of evaporation from their ponds must be thoroughly evaluated prior to their construction, and afterward, the advantages and disadvantages of the dam construction can be evaluated. The proposed approach is transferable and can be applied for similar settings along the Red Sea extension such as in the Eastern Desert of Egypt, Red Sea Hills in Saudi Arabia and in Sudan, and in different arid rift systems worldwide.

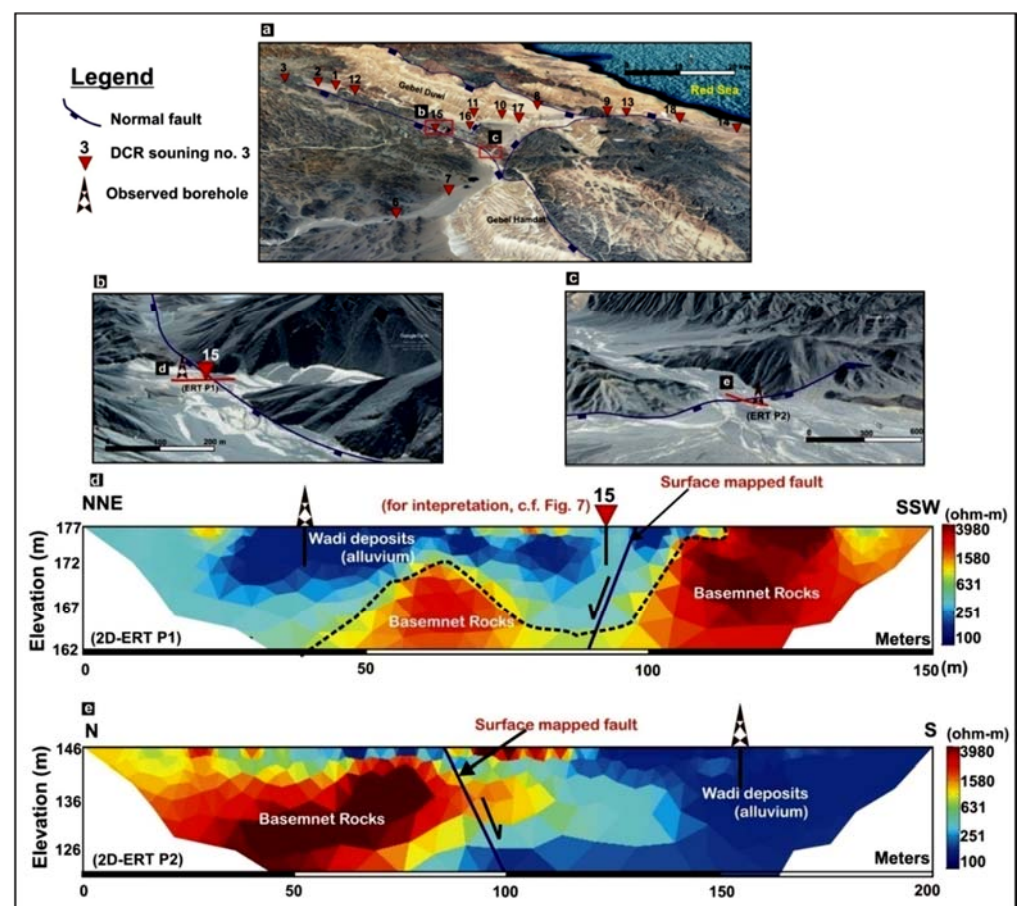


Figure 10. (a) Location map of geophysical measurements (1D- and 2D-ERTs) showing the areas being intercepted by structural aligned scarps and normal faults. (b,c) Location maps of selected 2D-ERTs P1 and P2 sites, respectively. (d,e) 2D-ERT inversion results of P1 and P2 sites, respectively, showing the subsurface geology and inferred faults related to observed surface faults.

5. Conclusions

The complexity of hydrological conditions prevails most of arid regions such as Wadi Al-Ambagi watershed, where observations and in situ measurements are simply not available. Data scarcity in such areas is the main delphinium for assessment of water resources at practical scales. This research can handle these challenges by the integration of RS, GIS, and DCR techniques which was very useful for the assessment of surface hydrological parameters as well as subsurface aquifer settings. This integration provides novel solutions for water management in structurally-controlled arid watersheds through

locating potential areas suitable for surface water harvesting into subsided blocks within the impermeable crystalline rocks. The estimated total discharge of a hypothetical 10 mm effective rainfall storm over the entire basin was approximately 15 million cubic meters, which exceeds the storage capacity of existing mitigation measures (dams and retention basins). Therefore, additional dams have been proposed in the subcatchments underlain by considerable alluvium and sedimentary thickness that can contain the flash-flood water and provide an effective groundwater aquifer. From geophysical point of view, the study proved that the joint use of advanced conventional and nonconventional inversion algorithms, where the inversion results were calibrated with borehole stratigraphy and regional structural settings, is crucial in the hydrogeological evaluation in dryland basins. This study includes the first joint application of RS and ERT techniques to demonstrate where new dams can be constructed to manage and replenish the flash floods and the aquifers, respectively. The utilized approach can be widely applied in similar watersheds in the Eastern Desert of Egypt, Saudi Arabia, and Sudan, as well as similar rift basins worldwide.

Author Contributions: Conceptualization, M.A. and A.Z.A.; methodology, M.A., D.R., and A.Z.A.; software M.A., D.R., and A.Z.A.; validation, M.A., M.E.B., A.O., and H.M.A.; formal analysis, M.A., M.E.B., D.R., and A.Z.A.; investigation, M.A., D.R., and A.Z.A.; resources, M.A., D.R., A.O., H.M.A., and A.Z.A.; data curation, M.A. and D.R.; writing—original draft preparation, M.A., D.R., and A.Z.A.; writing—review and editing, M.A., D.R., and A.Z.A.; visualization, M.A., A.Z.A., D.R., and M.E.B.; supervision, M.A. and M.E.B.; project administration, M.A. and A.Z.A.; funding acquisition, M.A., A.Z.A., A.O., and H.M.A. All authors have read and agreed to the published version of the manuscript.

Funding: This research was funded by the National Authority for Remote Sensing and Space Sciences (NARSS), Egypt.

Data Availability Statement: The data is available upon request from the first author.

Acknowledgments: Special thanks go to Günther (LIAG institute, Hannover, Germany), Basokur, and Akca (Ankara Uni. Turkey) and for the great support with inversion software during preparing this research.

Conflicts of Interest: The authors declare no conflict of interest.

References

- Ligi, M.; Bonatti, E.; Bosworth, W.; Cai, Y.; Cipriani, A.; Palmiotto, C.; Ronca, S.; Seyler, M. Birth of an ocean in the red sea: Oceanic-type basaltic melt intrusions precede continental rapture. *Gondwana Res.* **2018**, *54*, 150–160. [\[CrossRef\]](#)
- Sultan, M.; Yousef, A.F.; Metwally, S.E.; Becker, R.; Milewski, A.; Sauck, W.; Sturchio, N.C.; Mohamed, A.; Wagdy, A.; El Alfy, Z. Red sea rifting controls on aquifer distribution: Constraints from geochemical, geophysical, and remote sensing data. *GSA Bull.* **2011**, *123*, 911–924. [\[CrossRef\]](#)
- Ahmed, M.; Sauck, W.; Sultan, M.; Yan, E.; Soliman, F.; Rashed, M. Geophysical constraints on the hydrogeologic and structural settings of the Gulf of Suez rift-related basins: Case study from the El Qaa plain, Sinai, Egypt. *Surv. Geophys.* **2014**, *35*, 415–430. [\[CrossRef\]](#)
- Yousif, M.; Hussien, H.M.; Abotalib, A.Z. The respective roles of modern and paleo recharge to alluvium aquifers in continental rift basins: A case study from El Qaa plain, Sinai, Egypt. *Sci. Total Environ.* **2020**, *739*, 139927. [\[CrossRef\]](#)
- Abotalib, A.Z.; Mohamed, R.S. Surface evidences supporting a probable new concept for the river systems evolution in Egypt: A remote sensing overview. *Environ. Earth Sci.* **2013**, *69*, 1621–1635. [\[CrossRef\]](#)
- Bojar, A.; Fritz, H.; Kargl, S.; Unzog, W. Phanerozoic tectonothermal history of the Arabian–Nubian shield in the Eastern Desert of Egypt: Evidence from fission track and paleostress data. *J. Afr. Earth Sci.* **2002**, *34*, 191–202. [\[CrossRef\]](#)
- Elhebery, M.S.; Sultan, M.; Abu El-Leil, I.; Kehew, A.E.; Bekiet, M.H.; Abdel Shahid, I.; Soliman, N.M.; Abotalib, A.Z.; Emil, M. Paleozoic glaciation in NE Africa: Field and remote sensing-based evidence from the South Eastern Desert of Egypt. *Int. Geol. Rev.* **2020**, *62*, 1187–1204. [\[CrossRef\]](#)
- Abotalib, A.Z.; Heggy, E.; Scabbia, G.; Mazzoni, A. Groundwater dynamics in fossil fractured carbonate aquifers in Eastern Arabian Peninsula: A preliminary investigation. *J. Hydrol.* **2019**, *571*, 460–470. [\[CrossRef\]](#)
- Szymanski, E.; Stockli, D.F.; Johnson, P.R.; Hager, C. Thermochronometric evidence for diffuse extension and two-phase rifting within the Central Arabian margin of the Red Sea rift. *Tectonics* **2016**, *35*, 2863–2895. [\[CrossRef\]](#)

10. Elkadiri, R.; Manche, C.; Sultan, M.; Al-Dousari, A.; Uddin, S.; Chouinard, K.; Abotalib, A.Z. Development of a coupled spatiotemporal algal bloom model for coastal areas: A remote sensing and data mining-based approach. *IEEE J. Sel. Top. Appl. Earth Obs. Remote. Sens.* **2016**, *9*, 5159–5171. [[CrossRef](#)]
11. Rateb, A.; Abotalib, A.Z. Inferencing the land subsidence in the Nile Delta using Sentinel-1 satellites and GPS between 2015 and 2019. *Sci. Total Environ.* **2020**, *729*, 138868. [[CrossRef](#)]
12. Hegazy, D.; Abotalib, A.Z.; El-Bastawesy, M.; El-Said, M.A.; Melegy, A.; Garamoon, H. Geo-environmental impacts of hydrogeological setting and anthropogenic activities on water quality in the Quaternary aquifer southeast of the Nile Delta. *Egypt. J. Afr. Earth Sci.* **2020**, *172*, 103947. [[CrossRef](#)]
13. El Bastawesy, M.; Cherif, O.H.; Sultan, M. The geomorphological evidences of subsidence in the Nile Delta: Analysis of high resolution topographic DEM and multi-temporal satellite images. *J. Afr. Earth Sci.* **2017**, *136*, 252–261. [[CrossRef](#)]
14. El-Saadawy, O.; Gaber, A.; Othman, A.; Abotalib, A.Z.; El Bastawesy, M.; Attwa, M. Modeling flash floods and induced recharge into alluvial aquifers using multi-temporal remote sensing and electrical resistivity imaging. *Sustainability* **2020**, *12*, 10204. [[CrossRef](#)]
15. Wade, A.J.; Black, E.; Brayshaw, D.J.; El-Bastawesy, M.; Holmes, P.A.C.; Butterfield, D.; Nuimat, S.; Jamjoum, K. A model-based assessment of the effects of projected climate change on the water resources of Jordan. *Philos. Trans. R. Soc. Math. Phys. Eng. Sci.* **2010**, *368*, 5151–5172. [[CrossRef](#)]
16. Gabr, S.; El Bastawesy, M. Estimating the flash flood quantitative parameters affecting the oil-fields infrastructures in Ras Sudr, Sinai, Egypt, during the January 2010 event. *Egypt J. Remote. Sens. Space Sci.* **2015**, *18*, 137–149. [[CrossRef](#)]
17. El Bastawesy, M.; White, K.; Nasr, A. Integration of remote sensing and GIS for modelling flash floods in Wadi Hudain catchment, Egypt. *Hydrol. Process. Int. J.* **2009**, *23*, 1359–1368. [[CrossRef](#)]
18. Gabale, S.M.; Pawar, N.R. Quantitative morphometric analysis of AmbilOdha (Rivulet) in Pune, Maharashtra, India. *IOSR J. Environ. Sci. Toxicol. Food Technol.* **2015**, *9*, 41–48.
19. Kant, S.; Meshram, S.; Dohare, R.; Singh, S. Morphometric analysis of sonar sub-basin using SRTM data and geographical information system (GIS). *Afr. J. Agric. Res.* **2015**, *10*, 1401–1406.
20. Naghibi, S.A.; Pourghasemi, H.R.; Abbaspour, K. A comparison between ten advanced and soft computing models for groundwater qanat potential assessment in Iran using R and GIS. *Theor. Appl. Climatol.* **2018**, *131*, 967–984. [[CrossRef](#)]
21. Khakhar, M.; Ruparelia, J.P.; Vyas, A. Assessing groundwater vulnerability using GIS-Based DRASTIC model for Ahmedabad District, India. *Environ. Earth Sci.* **2017**, *76*, 1–18. [[CrossRef](#)]
22. Othman, A.; Abotalib, A.Z. Land subsidence triggered by groundwater withdrawal under hyper-arid conditions: Case study from Central Saudi Arabia. *Environ. Earth Sci.* **2019**, *78*, 243. [[CrossRef](#)]
23. Radwan, F.; Alazba, A.A.; Mossad, A. Watershed morphometric analysis of Wadi Baish Dam catchment area using integrated GIS-based approach. *Arab. J. Geosci.* **2017**, *10*, 1–11. [[CrossRef](#)]
24. Attwa, M.; Günther, T.; Grinat, M.; Binot, F. Transmissivity Estimation from Sounding Data of Holocene Tidal Deposits in the North Eastern Part of Cuxhaven, Germany. In Proceedings of the Near Surface 2009-15th EAGE European Meeting of Environmental and Engineering Geophysics, European Association of Geoscientists and Engineers (EAGE), Dublin, Ireland, 7–9 September 2009; p. cp-00111.
25. Maurya, P.K.; Rønde, V.K.; Fiandaca, G.; Balbarini, N.; Auken, E.; Bjerg, P.L.; Christiansen, A.V. Detailed landfill leachate plume mapping using 2D and 3D electrical resistivity tomography-with correlation to ionic strength measured in screens. *J. Appl. Geophys.* **2017**, *138*, 1–8. [[CrossRef](#)]
26. Attwa, M.; Günther, T. Application of spectral induced polarization (SIP) imaging for characterizing the near-surface geology: An environmental case study at Schillerslage, Germany. *Aust. J. Basic Appl. Sci.* **2012**, *6*, 693–701.
27. Revil, A.; Coperey, A.; Shao, Z.; Florsch, N.; Fabricius, I.L.; Deng, Y.; Delsman, J.R.; Pauw, P.S.; Karaoulis, M.; Louw, P.G.B.D.; et al. Complex conductivity of soils. water resources. *Research* **2017**, *53*, 7121–7147.
28. Anomohanran, O.; Orhiunu, M.E. Assessment of groundwater occurrence in Olomoro, Nigeria using borehole logging and electrical resistivity methods. *Arab. J. Geosci.* **2018**, *11*, 1–9. [[CrossRef](#)]
29. AL-Menshed, F.H.; Thabit, J.M. Comparison between VES and 2D imaging techniques for delineating subsurface plume of hydrocarbon contaminated water Southeast of Karbala City, Iraq. *Arab. J. Geosci.* **2018**, *11*, 1–9. [[CrossRef](#)]
30. Hermans, T.; Irving, J. Facies discrimination with electrical resistivity tomography using a probabilistic methodology: Effect of sensitivity and regularisation. *Near Surf. Geophys.* **2017**, *15*, 13–25. [[CrossRef](#)]
31. Attwa, M.; Gemail, K.S.; Eleraki, M. Use of salinity and resistivity measurements to study the coastal aquifer salinization in a semi-arid region: A case study in Northeast Nile Delta, Egypt. *Environ. Earth Sci.* **2016**, *75*, 784. [[CrossRef](#)]
32. Goebel, T.; Weingarten, M.; Chen, X.; Haffener, J.; Brodsky, E.E. The 2016 Mw5. 1 Fairview, Oklahoma earthquakes: Evidence for long-range poroelastic triggering at >40 km from fluid disposal wells. *Earth Planet. Sci. Lett.* **2017**, *472*, 50–61. [[CrossRef](#)]
33. Abotalib, A.Z.; Sultan, M.; Elkadiri, R. Groundwater processes in Saharan Africa: Implications for landscape evolution in arid environments. *Earth Sci. Rev.* **2016**, *156*, 108–136. [[CrossRef](#)]
34. Hussien, H.M.; Kehew, A.E.; Aggour, T.; Korany, E.; Abotalib, A.Z.; Hassanein, A.; Morsy, S. An integrated approach for identification of potential aquifer zones in structurally controlled terrain: Wadi Qena Basin, Egypt. *Catena* **2017**, *149*, 73–85. [[CrossRef](#)]

35. Yousif, M.; Sracek, O. Integration of geological investigations with multi-GIS data layers for water resources assessment in arid regions: El Ambagi Basin, Eastern Desert, Egypt. *Environ. Earth Sci.* **2016**, *75*, 1–25. [[CrossRef](#)]
36. Youssef, A.M.; Pradhan, B.; Gaber, A.; Buchroithner, M.F. Geomorphological hazard analysis along the Egyptian Red Sea coast between Safaga and Quseir. *Nat. Hazards Earth Syst. Sci.* **2009**, *9*, 751–766. [[CrossRef](#)]
37. Amer, R.; Kusky, T.; El Mezayen, A. Remote sensing detection of gold related alteration zones in Um Rus Area, Central Eastern Desert of Egypt. *Adv. Space Res.* **2012**, *49*, 121–134. [[CrossRef](#)]
38. El Ramly, M.F. The Occurrence of Gold in the Eastern Desert of Egypt. *Stud. Some Miner. Depos. Egypt Geol. Surv. Egypt* **1970**, 53–64.
39. Mohamed, L.; Sultan, M.; Ahmed, M.; Zaki, A.; Sauck, W.; Soliman, F.; Yan, E.; Elkadiri, R.; Abouelmagd, A. Structural controls on groundwater flow in basement terrains: Geophysical, remote sensing, and field investigations in Sinai. *Surv. Geophys.* **2015**, *36*, 717–742. [[CrossRef](#)]
40. Conoco. *Geological Map of Egypt, Scale. 1987, 1: 500,000*, 36; Egyptian Petroleum Authority: Cairo, Egypt, 1987.
41. Attwa, M.; Henaish, A. Regional structural mapping using a combined geological and geophysical approach—A preliminary study at Cairo-Suez District, Egypt. *J. Afr. Earth Sci.* **2018**, *144*, 104–121. [[CrossRef](#)]
42. Başokur, A.T. Automated 1D interpretation of resistivity soundings by simultaneous use of the direct and iterative methods. *Geophys. Prospect.* **1999**, *47*, 149–177. [[CrossRef](#)]
43. Başokur, A.T.; Akca, I.; Siyam, N.W. Hybrid genetic algorithms in view of the evolution theories with application for the electrical sounding method. *Geophys. Prospect.* **2007**, *55*, 393–406. [[CrossRef](#)]
44. Akça, I.; Basokur, A.T. Extraction of structure-based geoelectric models by hybrid genetic algorithms. *Geophysic* **2010**, *75*, F15–F22. [[CrossRef](#)]
45. Attwa, M.; Akca, I.; Basokur, A.T.; Günther, T. Structure-based geoelectrical models derived from genetic algorithms: A case study for hydrogeological investigations along Elbe River coastal area, Germany. *J. Appl. Geophys.* **2014**, *103*, 57–70. [[CrossRef](#)]
46. Attwa, M.; Basokur, A.T.; Akca, I. Hydraulic conductivity estimation using direct current (DC) sounding data: A case study in East Nile Delta, Egypt. *Hydrogeol. J.* **2014**, *22*, 1163–1178. [[CrossRef](#)]
47. Hellman, K.; Johansson, S.J.; Olsson, P.O.; Dahlin, T.D. Resistivity Inversion Software Comparison. In Proceedings of the Near Surface Geoscience 2016-22nd European Meeting of Environmental and Engineering Geophysics; European Association of Geoscientists and Engineers (EAGE), Barcelona, Spain, 4–8 September 2016; p. cp-00115.
48. Günther, T.; Rücker, C. A General Approach for Introducing Information into Inversion and Examples from Dc Resistivity Inversion. In Proceedings of the Near Surface 2006-12th EAGE European Meeting of Environmental and Engineering Geophysics, European Association of Geoscientists and Engineers (EAGE), Helsinki, Finland, 4–6 September 2006; p. cp-00060.
49. Rücker, C.; Günther, T.; Spitzer, K. Three-dimensional modelling and inversion of Dc resistivity data incorporating topography—I. modelling. *Geophys. J. Int.* **2006**, *166*, 495–505. [[CrossRef](#)]
50. Nicholson, S.E. Desert Hydrology. In *Encyclopedia of Hydrology and Lakes. Encyclopedia of Earth Science*; Springer: Dordrecht, The Netherlands, 1998; pp. 176–183.
51. Sharon, D. The distribution of rainfall in space and time in the Namib desert. *J. Climatol.* **1981**, *1*, 69–75. [[CrossRef](#)]
52. Maidment, D.R. GIS and Hydrologic Modeling. In *Environmental Modeling with GIS*; Goodchild, M.F., Parks, B.O., Eds.; Oxford University Press Inc.: New York, NY, USA, 1993; pp. 147–167.
53. Beven, K. Runoff Generation in Semi-Arid Areas. In *Dryland Rivers, Hydrology and Geomorphology of Semi-Arid Channels*; Bull, L.J., Kirkby, M.J., Eds.; John Wiley and Sons: Chichester, UK, 2002; pp. 57–105.
54. Cooke, R.; Brunsten, D.; Doornkamp, J.C. *Urban Geomorphology in Drylands*; Oxford University Press: Oxford, UK, 1982.
55. Mabbutt, J.A. *Desert Landforms*; MIT Press: Cambridge, MA, USA, 1979; p. 340.
56. Henaish, A.; Attwa, M. Internal structural architecture of a soft-linkage transfer zone using outcrop and DC resistivity data: Implications for preliminary engineering assessment. *Eng. Geol.* **2018**, *244*, 1–13. [[CrossRef](#)]
57. Milewski, A.; Sultan, M.; Yan, E.; Becker, R.; Abdeldayem, A.; Soliman, F.; Gelil, K.A. A remote sensing solution for estimating runoff and recharge in arid environments. *J. Hydrol.* **2009**, *373*, 1–14. [[CrossRef](#)]